

## Discovery of a High-Redshift ( $z=0.96$ ) Cluster of Galaxies Using a *FIRST* Wide-Angle Tailed Radio Source<sup>1</sup>

Elizabeth L. Blanton<sup>2,3,4</sup>, Michael D. Gregg<sup>5,6</sup>, David J. Helfand<sup>4,7</sup>, Robert H. Becker<sup>5,6</sup>, and Richard L. White<sup>8</sup>

### ABSTRACT

Using a combination of near-infrared and optical photometry, along with multi-object spectroscopy, we have confirmed the existence of a high-redshift cluster of galaxies at  $z = 0.96$ . The cluster was found using a wide-angle tailed radio source selected from the VLA *FIRST* survey as a cluster signpost. These types of radio sources are often found in clusters, and are thought to attain their C-shaped morphologies from the relative motion between the radio source host galaxy and the intracluster medium. We present optical/near-infrared color-magnitude diagrams which show a concentration of cluster galaxies in color space. We also include spectroscopic results obtained from the Keck II LRIS. Ten galaxies are confirmed at the cluster redshift, with a line-of-sight velocity dispersion of  $\sigma_{\parallel} = 530_{-90}^{+190}$  km s<sup>-1</sup>, typical of an Abell richness class 0 cluster. Using data from the *ROSAT* public archive, we limit the X-ray luminosity for the cluster to  $L_{X,bol} \lesssim 3 \times 10^{44}$  erg s<sup>-1</sup>, consistent with the value expected from the  $L_X - \sigma$  relation.

---

<sup>1</sup>Based in part on observations obtained at the W. M. Keck Observatory.

<sup>2</sup>*Chandra* Fellow

<sup>3</sup>Department of Astronomy, University of Virginia, P. O. Box 3818, Charlottesville, VA 22903; eblanton@virginia.edu

<sup>4</sup>Visiting Astronomer, Kitt Peak National Observatory, National Optical Astronomy Observatories, which is operated by the Association of Universities for Research in Astronomy, Inc., under cooperative agreement with the National Science Foundation

<sup>5</sup>Department of Physics, University of California at Davis, 1 Shields Avenue, Davis, CA 95616; gregg@igpp.ucllnl.org, bob@igpp.ucllnl.org

<sup>6</sup>Institute of Geophysics and Planetary Physics, Lawrence Livermore National Laboratory, L-413, P.O. Box 808, Livermore, CA 94550

<sup>7</sup>Columbia Astrophysics Laboratory, 550 West 120th St., New York, NY 10027; djh@astro.columbia.edu

<sup>8</sup>Space Telescope Science Institute, 3700 San Martin Dr., Baltimore, MD 21218; rlw@stsci.edu

## 1. Introduction

Clusters of galaxies trace the largest gravitationally-bound mass concentrations in the Universe; their epoch of formation, and thus their abundance as a function of redshift, is a strong constraint on  $\Omega_M$ . High-redshift clusters are very difficult to find – the faint optical magnitudes of the associated galaxies and the X-ray emission from the intracluster medium (ICM) will often be missed by current surveys at redshifts of  $z \approx 1$ . Any new clusters revealed at these distances add significantly to the few that are known, and are useful for studies of cosmology and galaxy evolution.

Using a unique method based on radio galaxy morphology, we have confirmed the existence of dozens of clusters with redshifts up to  $z = 0.85$  (Blanton et al. 2000, 2001). Bent double-lobed radio sources (particularly FR I-type sources [Fanaroff & Riley 1974], including wide-angle tails [WATs] and narrow-angle tails [NATs]) are thought to achieve their distinct “swept-back”, C-shaped morphologies as a result of interaction with dense gas in which they are embedded. The canonical model describes the radio source’s host galaxy as having a significant peculiar velocity relative to the cluster with which it is associated – the ram pressure of the dense ICM then pushes back the lobes of the radio source giving it a “bent” appearance (Owen & Rudnick 1976). Often, the host galaxies of WAT radio sources are cD ellipticals, thought to reside at the bottom of cluster potential wells, and are thus not expected to have significant peculiar velocities. An alternate explanation (Burns et al. 1994), posits bulk motion of the ICM as a result of a recent or ongoing cluster-cluster (or sub-cluster) merger. The ram pressure of the merging gas then bends the lobes. Either way, bent-double radio sources are often pointers to clusters, and they may be flags in particular for clusters that have recently formed or merged.

We have selected 384 bent-double (mostly WAT) radio sources from the first 3000 deg<sup>2</sup> of the VLA *FIRST* (Faint Images of the Radio Sky at Twenty-cm) survey (Becker, White, & Helfand 1995). Imaging and multi-slit mask spectroscopic follow-up on a moderate-to-high redshift subset of ten of these revealed eight clusters with redshifts as high as  $z = 0.85$  (Blanton et al. 2000). A complete (area- and magnitude-limited) low-redshift subset including 40 of the 384 objects was observed optically, and  $\sim 50\%$  of them were found to be in richness class Abell 0 or greater clusters (Blanton et al. 2001). The majority of the low-redshift bent doubles that are found in clusters, based on our optical richness measurements, are detected in the ROSAT All Sky Survey (five out of six detected for  $z < 0.2$ ). Those that are not found in clusters, based on our richness measurements, are not detected in the RASS (only one out of nine detected for  $z < 0.2$ ). In other words, the combination of radio and optical data gives us a very clear indication for the presence, or lack of, a cluster, as confirmed with X-ray observations.

In order to identify high- $z$  candidates, we obtained  $R$ -band images of fields surrounding bent doubles that were blank to the limit of the Digitized Sky Survey (DSS). Some of these had no optical identifications even down to the limit of our images ( $m_R \sim 22 - 23$ ). We then performed near-infrared (NIR) observations at the positions of these sources in hopes of uncovering very red, high- $z$  cluster galaxies.

NIR observations have been successful in the past in identifying high- $z$  clusters. Stanford et al. (1997, 2001) found one of the most distant clusters known at  $z = 1.27$  using NIR and optical imaging, while Rosati et al. (1999) used a combination of X-ray, NIR, and optical observations to confirm the existence of a cluster at  $z = 1.26$  that may be part of a superstructure including the Stanford et al. (1997) cluster. Using the NIR alone, or in conjunction with radio and/or X-ray data, gives the potential for locating clusters that are at such high- $z$  they would be missed by all but the deepest optical observations. Recently, Gladders & Yee (2000) have performed a high-redshift cluster search by using optical and NIR photometry and identifying clusters by their “red sequence,” or clustering on a color-magnitude diagram. Chapman et al. (2000) have used a combination of radio observations with optical and NIR photometry to identify likely clusters at redshifts greater than 0.8.

Here we present optical and NIR observations taken at the position of the bent-double radio source, BD1137+3000. A combination of imaging and spectroscopy confirms that this source is located in a distant cluster of galaxies with a redshift  $z = 0.96$ .

We assume  $H_0 = 70 \text{ km s}^{-1} \text{ Mpc}^{-1}$ ,  $\Omega_M = 0.3$ , and  $\Omega_\Lambda = 0.7$  throughout.

## 2. BD1137+3000: Radio Data

The radio source is detected in the *FIRST* survey as a three component object, including a core and two lobes (FIRST J113733.6+300009, FIRST J113734.0+300002, and FIRST J113732.8+300003). The position of the core is  $\alpha = 11\text{h } 37\text{m } 33.62\text{s}$ ,  $\delta = +30^\circ 00' 9''.5$ . The source is clearly bent with an opening angle between the two lobes of  $\sim 80^\circ$ . The size of the source, measured from the outer edge of one lobe to the core and out to the outer edge of the other lobe is  $30''$  (240 kpc). The total flux density, as measured by *FIRST* is 9.1 mJy. The southeast lobe is the brightest of the three components, with a flux density of 4.1 mJy. The core has a comparable flux density (3.8 mJy), while the southwest lobe is 1.2 mJy. It is difficult to classify the source as an FR I or II based on its morphology. The southeast lobe is bright at the end of the lobe (typical of an FR II source). The southwest lobe brightens approximately halfway between the core and the edge of the lobe, bends at this bright area, and then fades toward the edge of the lobe (typical of an FR I source). We expect that there is additional extended emission related to the source that is not seen because (1) there is surface brightness dimming  $\propto (1+z)^4$  and (2) it is resolved out by the high resolution of the *FIRST* images. The flux density measured from the low-resolution NRAO VLA Sky Survey (*NVSS*; Condon et al. 1997), which resolves out less extended emission, 9.8 mJy, is slightly higher than the *FIRST* value. Using the *NVSS* flux density value, and assuming  $P \propto \nu^{-\alpha}$  with  $\alpha = 0.8$ , the radio power of the source at 1440 MHz is  $P_{1440} = 4.0 \times 10^{25} \text{ W Hz}^{-1}$ . This power is slightly below the FR I/II break for radio galaxies (Fanaroff & Riley 1974), and is typical of the class of bent double radio sources known as wide-angle tails (WATs; O’Donoghue et al. 1993) which are very often associated with cD galaxies in the centers of clusters. An overlay of the *FIRST* radio contours onto a Keck near-infrared camera (NIRC) image in the  $K'$  filter of the cluster center is

shown in Figure 1. The figure is 280 kpc on a side for our assumed cosmology. The radio contours are logarithmically spaced in the range 0.45 to 4.0 mJy. The radio core is coincident with an elliptical galaxy, as seen in the near-infrared image. This NIR image, which covers only the inner 35'' square region of the cluster, is used for display purposes only in this paper. We include analysis of NIR data from the KPNO 2.1m telescope covering a much wider field of view in the following section.

### 3. Optical/NIR Imaging Data and Reductions

Optical data taken in the R-band at the KPNO 2.1m under partly cloudy conditions on UT 6 April 1997 revealed no identification for the radio galaxy to a limit of  $R \approx 22$ . This motivated us to observe the object in the NIR, and later to reobserve it to deeper limits in the optical under photometric conditions.

#### 3.1. NIR

BD1137+30 was observed with IRIM at the KPNO 2.1m on UT 25 and 26 May 1997; the image scale was 1''09/pixel. Observations were taken in a 16-point grid pattern. The total exposure in the  $K$ -band was 64 minutes (64 frames of 4×15 s coadds), and that in the  $J$ -band was 32 minutes (16 frames of 4×30 s coadds). The seeing was approximately 1''6 for the  $J$ -band image and 1''7 for the  $K$ -band image. A non-linearity correction was applied to the data to account for the changing response of the instrument when high fluxes are encountered. The correction was kindly provided by F. R. Chromey, derived from a non-linearity sequence taken the night immediately following our run, and amounted to a 3.3% correction at 30,000 counts. The data were corrected for the effects of dark current and flat fields using IRAF. The flat fields were constructed for each band by median combining the dithered target images and rejecting the objects contained therein. These types of flats were superior to dome flats (which we also constructed). The images were then processed with the IRAF contributed package DIMSUM<sup>9</sup>. We used DIMSUM to sky-subtract the data by using the sky derived from eight images taken immediately before and after each frame. The frames were then aligned and combined to produce a 'first pass' combined image. During this first pass, object masks were constructed for the frames to help eliminate object residuals in the final combined image. A 'mask pass' run incorporated these masks and produced the final combined image. We modified DIMSUM to attain better alignment of the images before combining them. The final mosaicked image reduced the image scale by a factor of four (to 0''27/pixel – see Stanford, Eisenhardt, & Dickinson (1995)). During the reduction process, a few bad frames were identified and rejected, leaving us with a total of 30 min in the  $J$ -band and 56 min in the  $K$ -band.

---

<sup>9</sup>Deep Infrared Mosaicking Software, um... Created by P. Eisenhardt, M. Dickinson, S. A. Stanford, & J. Ward

The final ‘mask pass’ combined images were normalized so that the counts are counts per second. UKIRT faint standards were used to derive the photometry.

### 3.2. Optical

A total exposure in the  $R$ -band of 7200 s ( $6 \times 1200$ s) at the MDM 1.3m telescope with the Templeton CCD obtained on UT 21 May 1998 was kindly provided by J. Kemp. This setup produced an image scale of  $0''.5/\text{pixel}$ . The night was photometric and the seeing was approximately  $1''.2 - 1''.3$ . The data were processed following standard IRAF procedures to remove the effects of the bias and flat field. The images were aligned and median-combined with cosmic rays rejected. The Landolt standard field PG1323 was used to calibrate the data.

## 4. Photometry / Image Analysis

FOCAS was used to measure magnitudes for the standard stars and objects in the target fields for the NIR and optical data. FOCAS ‘total’ magnitudes were measured for the standards. The error for the optical photometry, estimated from the scatter in the offset between the measured and Landolt-catalogued magnitudes for five stars in PG1323, is 0.04 mag. The error in the NIR magnitudes, estimated from the difference in the zero point derived for the two nights, is 0.1 mag.

Aperture magnitudes were measured for objects in the target field. To assure that we were measuring the same physical aperture in each band, as well as to make the analysis more straightforward, adjustments were made to the final  $R$ ,  $J$ , and  $K$  images. They were all scaled to have the same pixel scale ( $0''.5/\text{pix}$ ) and the same orientation (N up, E to the left). The  $R$  and  $J$  images were smoothed with a Gaussian to match the seeing in the  $K$ -band image (the worst of the three, with  $1''.7$ ). We then used FOCAS to measure magnitudes within an aperture with a diameter equal to  $2 \times \text{FWHM}$  ( $3''.4 = 6.8$  pixels). This is close to a total magnitude and will measure the same part of the galaxy in each of the bands. At  $z = 0.96$  (see §6), this aperture corresponds to 27 kpc for our assumed cosmology. The detection limit was  $2.5\sigma$  above sky and the minimum area was  $12 \text{ pixels}^2 = 2.9 \text{ arcsec}^2$  (the square of the FWHM). The sky was calculated by taking the average pixel value in a square annulus (default width 3 pixels) some buffer distance (default 2 pixels) away from the edge of the objects’ last isophotes. A small difference in the sky value had a very significant effect on faint objects. To assure that we weren’t including galaxy light in the sky subtraction, since many of the galaxies are very close together, we increased the buffer distance until the change in distance no longer affected the measured aperture magnitude (i.e., the sky value was no longer changing). We used a buffer of 15 pixels in  $R$  and 20 pixels in  $J$  and  $K$ .

The aperture magnitudes, measured as described above, for the radio source counterpart are  $22.90 \pm 0.04$ ,  $19.46 \pm 0.1$ , and  $17.78 \pm 0.1$ , in  $R$ ,  $J$ , and  $K$ , respectively. This gives colors of  $(R - K) = 5.12 \pm 0.11$ ,  $(J - K) = 1.68 \pm 0.14$ , and  $(R - J) = 3.44 \pm 0.11$ . The absolute magnitude of the host

galaxy is  $M_V = -22.29$ , assuming no evolution, a redshift  $z = 0.96$  (see §6), and a  $K$ -correction from Coleman, Wu, & Weedman (1980). This is typical of a bright elliptical galaxy, but fainter than a cD.

## 5. Color-Magnitude Diagrams

Color magnitude diagrams (CMDs) were constructed for objects in the entire 15.6 arcmin<sup>2</sup> field as well as for only the objects found within a 1' radius aperture (480 kpc at  $z = 0.96$ , see §6) from the radio source. No separation was made between stars and galaxies (all were included). At magnitudes close to that of the radio source, star/galaxy separation is very difficult, and not very important since number counts at these faint magnitudes are dominated by galaxies. The CMDs are presented in Figures 2 and 3. The top panels include the objects within 1' from the radio source, while the bottom panels include the objects from the entire field. The objects that are confirmed to be at the cluster redshift (see §6) are circled. Three obvious, foreground stars are seen in the diagrams – the three blue objects apparent in the CMDs constructed from the objects within one arcmin of the radio source. There is a much larger range in the colors of objects when looking at the CMDs for the whole field. The objects in the 1' radius aperture have less scatter (they are much more concentrated on the diagram) than those in the whole field, and are redder, consistent with membership in a distant cluster. Most of the objects within 1' from the radio source have colors in the range  $4 < (R - K) < 6$  and  $1.5 < (J - K) < 2.5$ . Comparing the CMDs to those presented in Stanford, Eisenhardt, & Dickinson (1998), which includes diagrams for 19 clusters from  $z = 0.3 - 0.9$ , and Stanford et al. (1997), which displays a CMD for a  $z = 1.27$  cluster, suggests that this cluster has a redshift between  $z = 0.9$  and 1.27, and closer to 0.9.

The  $R$ -band and  $K$ -band images are presented in Figure 4 and 5. Objects that were detected with at least  $2.5\sigma$  significance in both  $R$  and  $K$ , with a minimum area of 12 pixels<sup>2</sup> (2.9 arcsec<sup>2</sup>), and that have  $4 < (R - K) < 6$  are circled. Spectroscopically confirmed cluster members (see §6) are labeled with letters and numbers; details for these objects are given in Table 1. The radio source host galaxy is marked 'A'. Source 'C' was detected at only  $2\sigma$  in the  $R$ -band, and was not detected in the  $J$ -band, but is circled because it has a measured redshift.

## 6. Spectroscopy

### 6.1. Long-slit Observation

A long-slit observation ( $2 \times 30$  min.) of the cluster that included the radio counterpart and two other galaxies was made at the Keck II 10m telescope with the Low Resolution Imaging Spectrometer (LRIS; Oke et al. 1995) on 13 April 1998. The spectra were corrected for bias and flat field effects using standard IRAF procedures. They were wavelength calibrated using comparison

Ne + Ar spectra and flux calibrated using a standard star (Feige 34). Redshifts were derived from cross-correlating the spectra with an elliptical galaxy template (M32 shifted to the rest frame).

## 6.2. Multi-slit Mask Observation

A multi-slit mask observation of the field surrounding the radio source was made at the Keck II 10m telescope with LRIS on 29 May 2001. The field was observed for a total exposure of 60 min. ( $3 \times 20$  min.). We reduced the data from the LRIS-R, which was used with a 150 lines  $\text{mm}^{-1}$  grating. The central wavelength was 8495 Å, the dispersion was 4.8 Å/pix, and the pixel scale was 0.2109 arcsec/pix. Objects were chosen for the slit mask based on their ( $R - K$ ) colors. Objects that had  $4 < (R - K) < 6$  were candidates for inclusion on the mask, since they provide us the best opportunity of confirming galaxies at redshifts  $z \approx 1$ . The mask included a total of twelve program object slits.

The data were reduced following standard IRAF procedures. The frames were corrected for bias using the overscan region. An internal halogen flat taken through the mask following the data frames was used to correct for flat field effects. The three object frames were then aligned and combined with cosmic rays rejected.

Spectra were successfully extracted for seven of the program objects; the remaining five were too faint for successful extractions. The spectra were wavelength-calibrated using comparison spectra of Hg + Ar lamps. Redshifts were initially estimated by identifying a few obvious lines, including the Ca II H+K break, and the [O II]  $\lambda 3727$  and [O III]  $\lambda\lambda 4959, 5007$  emission lines. The spectra were then Fourier cross-correlated with an elliptical galaxy template (M32 shifted to the rest frame) using FXCOR in IRAF. The errors in the redshifts are computed in FXCOR and are based on the fitted peak height and the antisymmetric noise, or “r-value” (Tonry & Davis 1979). The average (mean) error for the redshifts from both the long-slit and multi-slit mask observations is  $150 \text{ km s}^{-1}$ .

## 6.3. Spectroscopic Results

All ten spectra that were successfully extracted had redshifts in the range  $0.950 < z < 0.965$ , giving us a 100% success rate of identifying cluster galaxies based on their NIR/optical colors. The objects and their redshifts are listed in Table 1. The spectrum of the radio host galaxy is shown in Figure 6, and is typical of an elliptical galaxy. The spectrum has been smoothed with an 11 pixel boxcar. We calculated the line-of-sight velocity dispersion using  $\sigma_{\parallel} = \sqrt{(N - 1)^{-1} \sum_{i=1}^N \Delta v_i^2}$ , where  $\Delta v_i = c(z_i - \bar{z})/(1 + \bar{z})$ . The 68% confidence uncertainty is calculated following Danese, De Zotti, and di Tullio (1980), and includes errors due to the small number of member galaxies in the field and the measurement errors. We find  $\sigma_{\parallel} = 530_{-90}^{+190} \text{ km s}^{-1}$ . This is a typical value for an Abell richness class 0 cluster (Lubin & Bahcall 1993).

## 7. Limit on the X-ray Luminosity

An observation in the *ROSAT* public data archive serendipitously includes the position of BD1137+3000. The *ROSAT* PSPC observation was centered at  $\alpha = 11\text{h}36\text{m}33.6\text{s}$ ,  $\delta = +29^\circ48'00''.0$  leaving the position of the bent-double radio source  $17''.8$  from the center, very close to the inner support structure of the PSPC. The observation was performed on 1991 May 30, for a total duration of 33447 seconds.

We processed the data using the Snowden routines<sup>10</sup> (Snowden et al. 1994) which correct for exposure, vignetting, variations in the detector quantum efficiency and non-cosmic background components. After applying these routines, 17884 seconds worth of good data remained. We extracted the X-ray count rate within a  $1'$  (480 kpc) radius aperture centered on the position of the radio source, and took background from two large circular apertures with similar offsets from the center of the PSPC field as the source region. The source region contained counts above the background at the  $2.1\sigma$  level, with a 90% confidence upper limit on the count rate of  $1.1 \times 10^{-3}$  ct  $\text{s}^{-1}$  in the 0.4 – 2.0 keV energy band. We converted this to a bolometric X-ray luminosity with PIMMS, using a model including Galactic absorption of  $N_H = 1.93 \times 10^{20}$   $\text{erg cm}^{-2}$  (Dickey & Lockman 1990), a Raymond-Smith plasma with a temperature of 2.4 keV (estimated from the  $\sigma - T$  relation [Lubin & Bahcall (1993)]), a chemical abundance of 0.4 times the solar value, and a redshift of  $z = 0.96$ . The upper limit on the bolometric X-ray luminosity is then  $L_{X,bol} \lesssim 3 \times 10^{44}$   $\text{erg s}^{-1}$ , which is consistent with the values expected from the  $L_x - \sigma$  relation ( $3 \times 10^{44}$   $\text{erg s}^{-1}$  [Edge & Stewart 1991];  $5 \times 10^{43}$   $\text{erg s}^{-1}$  [Borgani et al. 1999]). *Chandra* and *XMM-Newton* observations are planned to confirm the presence of an X-ray emitting ICM in this cluster, and to study it in more detail.

## 8. Conclusions

We have provided evidence at optical and near-infrared wavelengths for a high-redshift cluster of galaxies associated with a wide-angle tailed radio galaxy at  $z = 0.96$ . Color-magnitude diagrams reveal an over-density of red objects near the radio source with colors consistent with elliptical galaxies at this redshift. Objects are clustered on the color-magnitude diagrams in the range  $4 < (R - K) < 6$  and  $1.5 < (J - K) < 2.5$ .

Using spectroscopy from the Keck II LRIS, we have confirmed a total of ten galaxies at the cluster redshift. The line-of-sight velocity dispersion is  $\sigma_{\parallel} = 530^{+190}_{-90}$   $\text{km s}^{-1}$ , typical of an Abell richness class 0 cluster. Using data from the *ROSAT* public archive, we limited the cluster’s bolometric X-ray luminosity to  $L_{X,bol} \lesssim 3 \times 10^{44}$   $\text{erg s}^{-1}$ , which is consistent with the value expected from the  $L_X - \sigma$  relation.

---

<sup>10</sup>“Cookbook for Analysis Procedures for *ROSAT* XRT/PSPC Observations of Extended Objects and the Diffuse Background”, S. L. Snowden (1994), with support from the USRSDC



The majority of high-redshift clusters found in traditional X-ray and optical surveys select the most X-ray luminous and optically rich clusters. The radio selection technique employed here is an important complement to those methods, in part because it can locate high- $z$  clusters with a wide range of X-ray luminosities and optical richnesses, thus aiding in the study of galaxy evolution and cluster formation.

E. L. B. thanks Adam Stanford and Craig Sarazin for helpful discussions regarding the NIR and X-ray data reduction, respectively. Support for E. L. B. was provided by NASA through the *Chandra* Fellowship Program, grant award number PF1-20017, under NASA contract number NAS8-39073. Part of the work reported here was done at the Institute of Geophysics and Planetary Physics, under the auspices of the US Department of Energy by Lawrence Livermore National Laboratory under contract W-7405-Eng-48. Support for M. D. G. was provided by a grant from the National Science Foundation (AST-99-70884). The *FIRST* project is supported by grants from the National Geographic Society, the National Science Foundation (AST 00-98259 and AST 00-98355), NASA (NAG 5-6035), NATO, IGPP, Columbia University, and Sun Microsystems.

## REFERENCES

- Blanton, E. L., Gregg, M. D., Helfand, D. J., Becker, R. H., & Leighly, K. M. 2001, *AJ* 121, 2915
- Blanton, E. L., Gregg, M. D., Helfand, D. J., Becker, R. H., & White, R. L. 2000, *ApJ*, 531, 118
- Burns, J. O., Rhee, G., Owen, F. N., & Pinkney, J. 1994, *ApJ*, 423, 94
- Becker, R. H., White, R. L., & Helfand, D. J. 1995, *ApJ*, 450, 559
- Borgani, S., Girardi, M., Carlberg, R. G., Yee, H. K. C., & Ellingson, E. 1999, *ApJ*, 527, 561
- Chapman, S. C., McCarthy, P. J., & Persson, S. E. 2000, *AJ*, 120, 1612
- Coleman, G. D., Wu, C.-C., & Weedman, D. W. 1980, *ApJS*, 43, 393
- Condon, J. J., Cotton, W. D., Greisen, E. W., Yin, Q. F., Perley, R. A., Taylor, G. B., & Broderick, J. J. 1997, *AJ*, 115, 1693
- Danese, L., De Zotti, G., & di Tullio, G. 1980, *A&A*, 82, 322
- Dickey, J. M., & Lockman, F. J. 1990, *ARA&A*, 28, 215
- Edge, A. C., & Stewart, G. C. 1991, *MNRAS*, 252, 414
- Fanaroff, B. L., & Riley, J. M. 1974, *MNRAS*, 167, 31L
- Gladders, M. D., & Yee, H. K. C. 2000, *AJ*, 120, 2148
- Lubin, L. M., & Bahcall, N. A. 1993, *ApJ*, 415, L17
- O'Donoghue, A. A., Eilek, J. A., & Owen, F. N. 1993, *ApJ*, 408, 428
- Oke, J.B. et al. 1995, *PASP*, 107, 375
- Owen, F. N., & Rudnick, L. 1976, *ApJ*, 205, L1

- Rosati, P., Stanford, S. A., Eisenhardt, P. R., Elston, R., Spinrad, H., Stern, D., & Dey, A. 1999, AJ, 118, 76
- Snowden, S. L., McCammon, D., Burrows, D. N., & Mendenhall, J. A. 1994, ApJ, 424, 714
- Stanford, S. A., Eisenhardt, P. R., & Dickinson, M. 1995, ApJ, 450, 512
- Stanford, S. A., Holden, B., Rosati, P., Tozzi, P., Borgani, S., Eisenhardt, P. R., & Spinrad, H. 2001, ApJ, 552, 504
- Stanford, S. A., Elston, R., Eisenhardt, P. R., Spinrad, H., Stern, D., Dey, A. 1997, AJ, 114, 2232
- Stanford, S. A., Eisenhardt, P. R., & Dickinson, M. 1998, ApJ, 492, 461
- Tonry, J. & Davis, M. 1979, AJ, 84, 10

Table 1. Photometry and Redshifts for Confirmed Cluster Members

id	RA(J2000)	Dec(J2000)	$m_R$	$m_J$	$m_K$	$J - K$	$R - K$	$z$
A	11:37:33.74	30:00:10.5	22.90	19.46	17.78	1.68	5.12	0.9529
B	11:37:33.59	30:00:07.6	23.57	20.17	17.90	2.27	5.67	0.9524
C	11:37:33.34	30:00:02.8	24.28	...	18.91	...	5.37	0.9551
2	11:37:24.70	29:59:56.7	23.06	20.53	18.94	1.59	4.12	0.9591
5	11:37:32.16	30:00:11.4	22.92	19.83	17.71	2.12	5.21	0.9506
6	11:37:33.16	30:00:09.1	23.46	20.19	18.24	1.95	5.22	0.9571
7	11:37:35.18	29:59:51.5	23.38	20.65	18.78	1.87	4.59	0.9621
9	11:37:37.65	30:00:36.7	22.55	19.55	17.53	2.02	5.01	0.9582
10	11:37:38.34	30:00:06.2	22.43	19.23	17.67	1.56	4.76	0.9556
11	11:37:40.63	29:59:52.5	22.83	19.40	17.42	1.98	5.42	0.9564

Note. — The redshifts for galaxies A, B, and C were determined from the longslit observation; the redshifts for the remaining galaxies were derived from the slitmask observation. The radio source host galaxy is source A. Source C was not detected in the  $R$ -band at  $2.5\sigma$ ,  $m_R$  for this galaxy is given at the  $2\sigma$  level. It was not detected in the  $J$ -band.

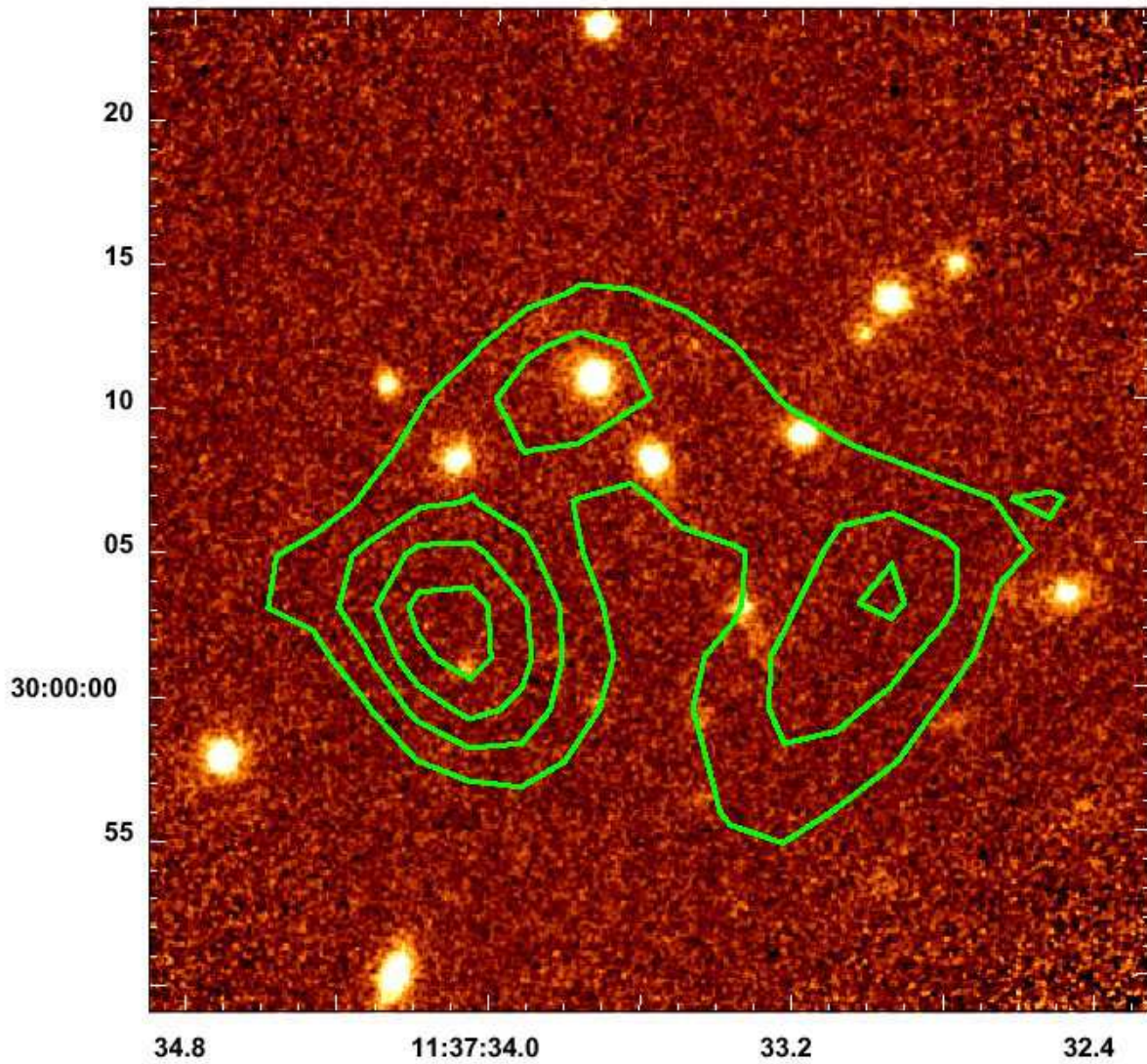


Fig. 1.— Overlay of the *FIRST* 20cm radio contours onto a  $K'$ -band image taken with the Keck NIRC. The contours are logarithmically spaced in the range 0.45 to 4.0 mJy. With our assumed cosmology, the figure is  $280 \times 280$  kpc.

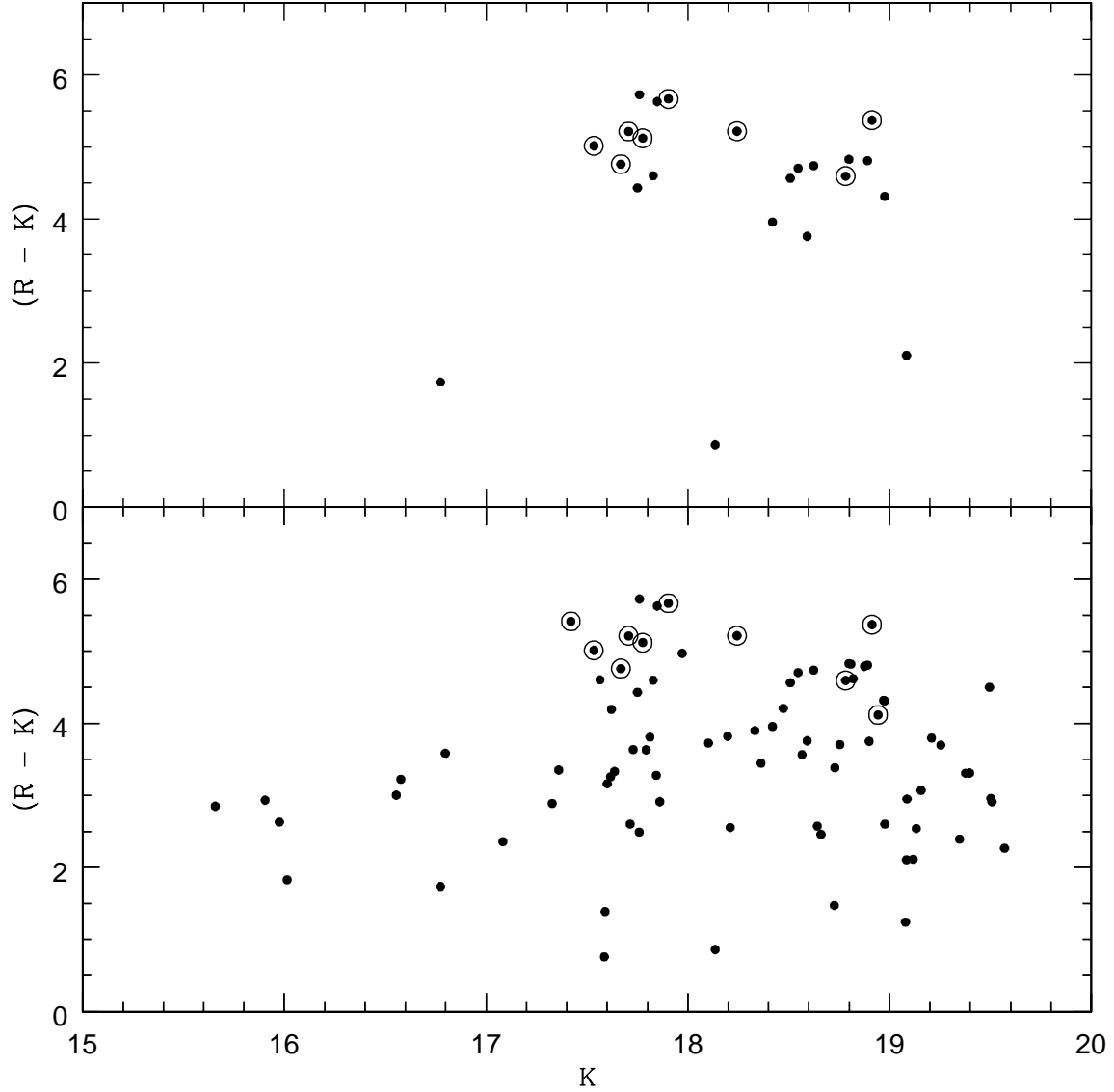


Fig. 2.—  $K$  vs.  $(R - K)$  color-magnitude diagram. The top panel includes the objects within a  $1'$  radius from the radio source, while the bottom panel includes the objects in the entire  $15.6 \text{ arcmin}^2$  field. There is a concentration of objects with  $4 < R - K < 6$  that are likely cluster members. Spectroscopically confirmed cluster members are circled.

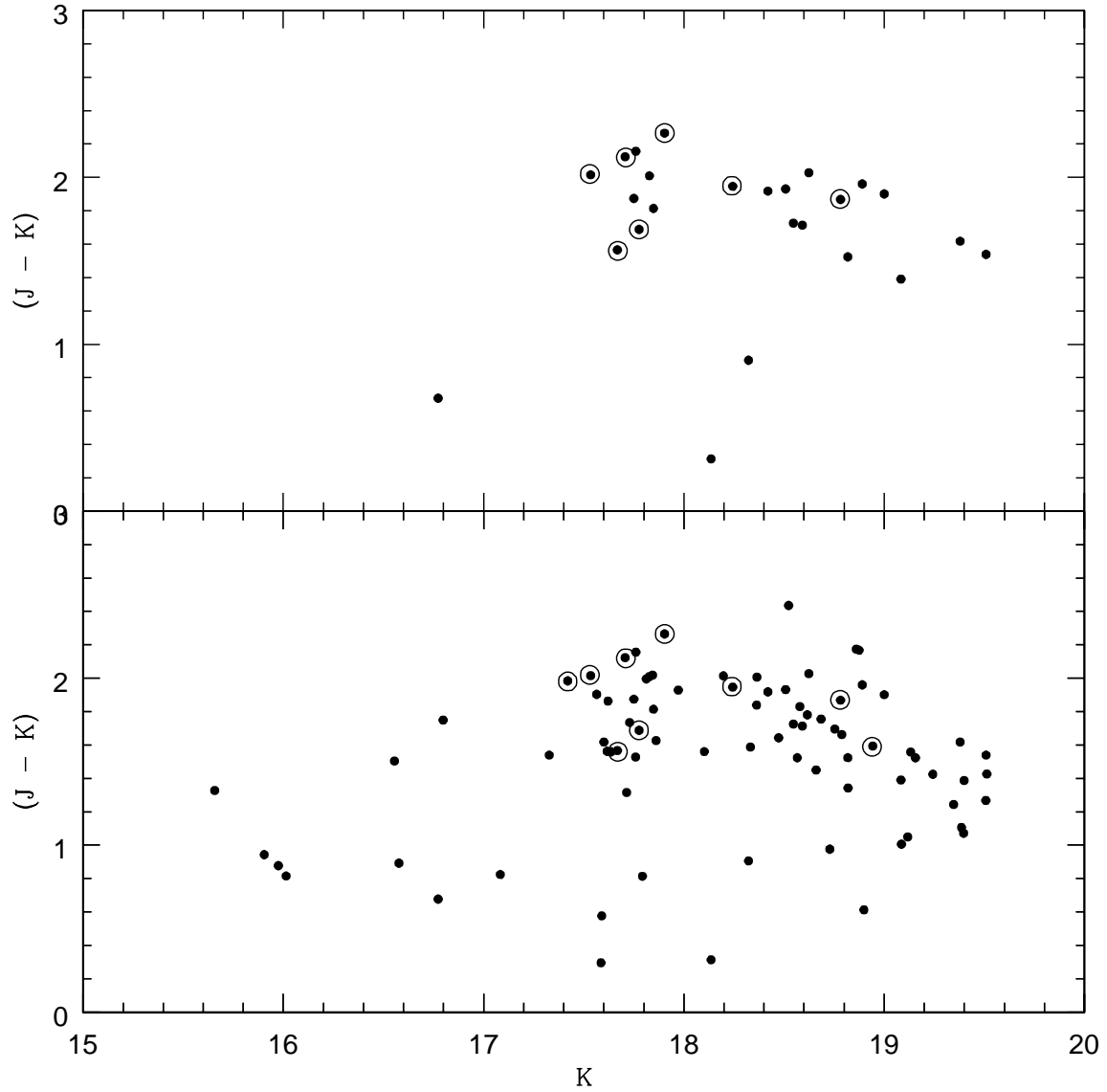


Fig. 3.—  $K$  vs.  $(J - K)$  color-magnitude diagram. As in Figure 2, the top panel includes only the objects within a  $1'$  radius from the radio source, and the bottom panel includes the objects in the entire  $15.6 \text{ arcmin}^2$  field. Probable cluster members have approximately  $1.5 < J - K < 2.5$ . Spectroscopically confirmed members are circled.

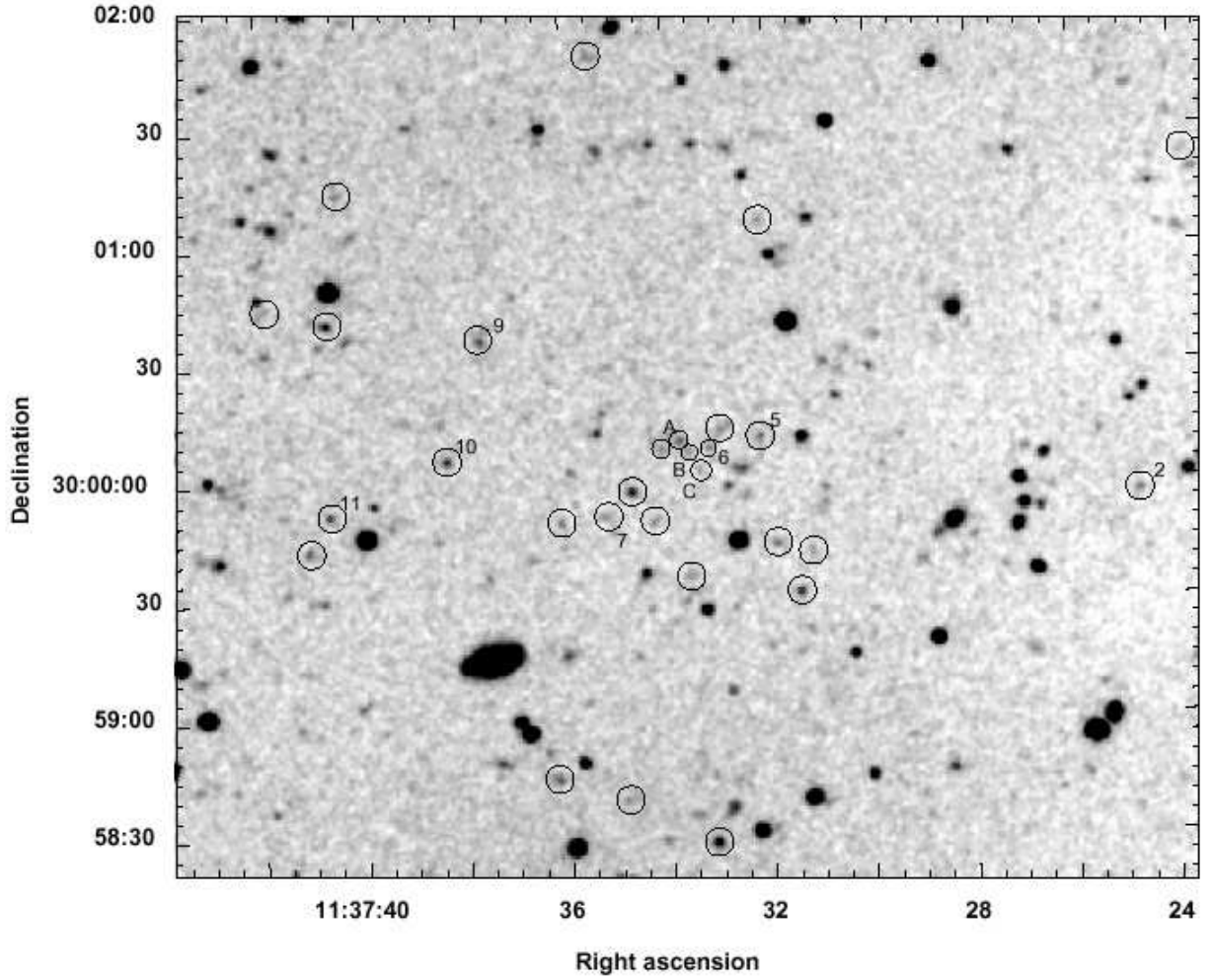


Fig. 4.—  $R$ -band image from the MDM 1.3m telescope. Objects with  $4 < R - K < 6$  are circled, and are likely cluster members. Spectroscopically confirmed members are labeled with letters and numbers; details for these objects are given in Table 1. The radio host galaxy is marked 'A'.

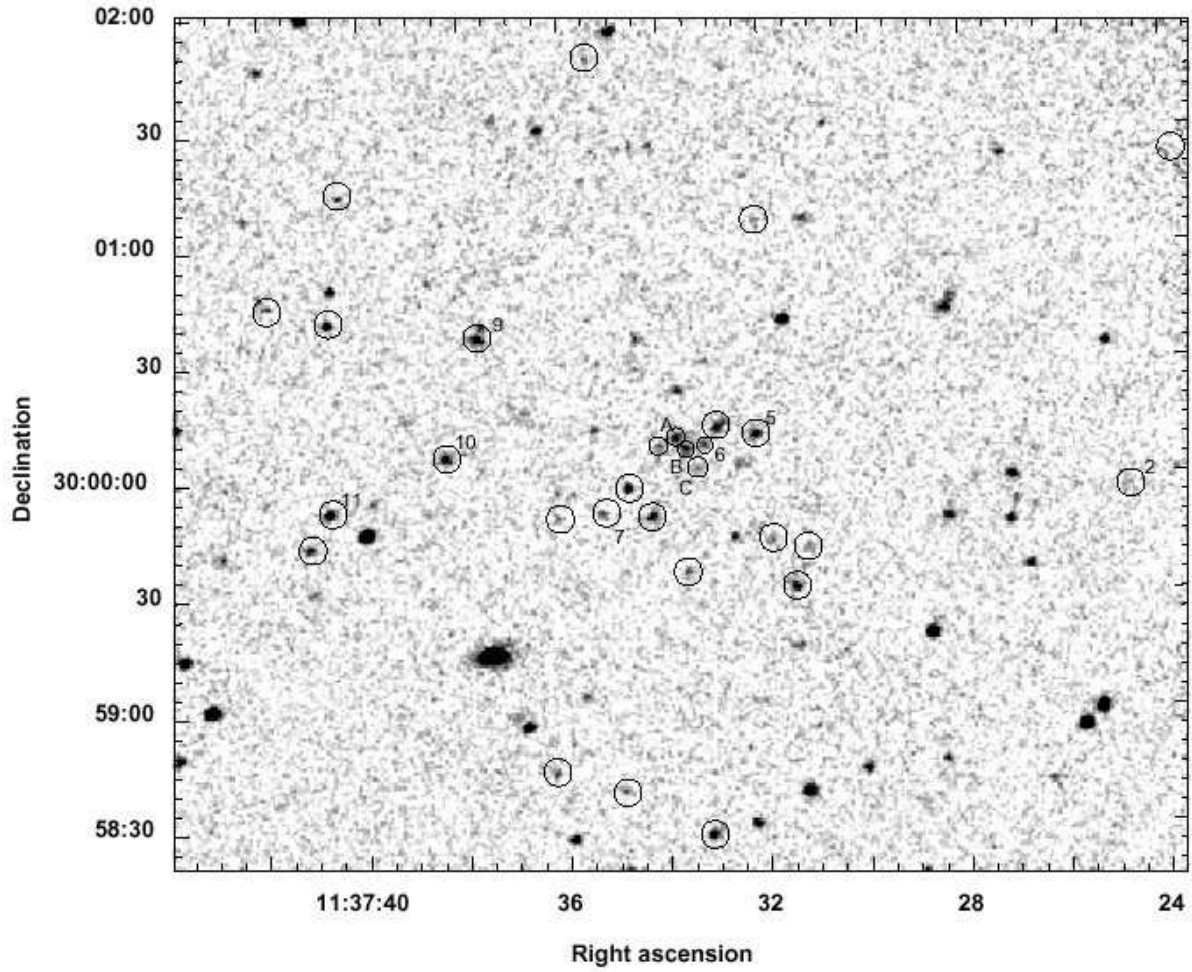


Fig. 5.— *K*-band image from the KPNO 2.1m telescope with the IRIM detector. Image labels are as described in Figure 4.



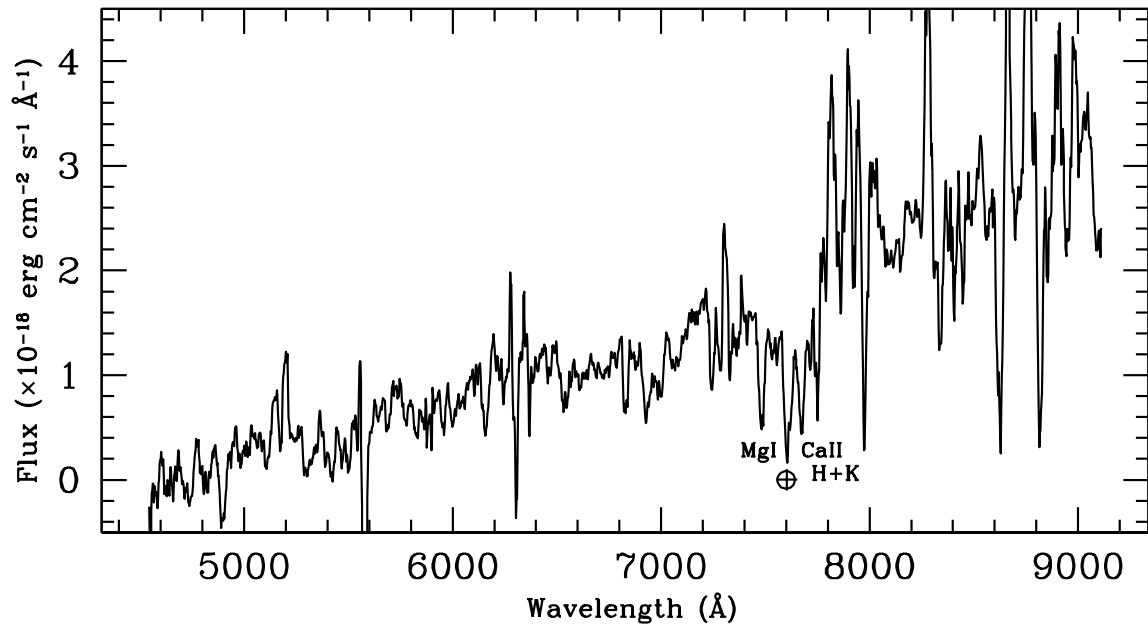


Fig. 6.— Keck II LRIS spectrum of the radio source host galaxy. The spectrum has been smoothed with an 11 pixel boxcar. The absorption features are typical of an elliptical galaxy.